

Revealing the traces of histogram equalisation in digital images

ISSN 1751-9659
 Received on 9th September 2017
 Revised 26th November 2017
 Accepted on 10th December 2017
 E-First on 18th January 2018
 doi: 10.1049/iet-ipr.2017.0992
 www.ietdl.org

Zeeshan Akhtar¹ ✉, Ekram Khan²

¹Department Electrical Engineering, Indian Institutes of Technology, Kanpur, India

²Department of Electronics Engineering, Zakir Husain College of Engineering and Technology, Aligarh Muslim University, Aligarh, India

✉ E-mail: zeeshan@iitk.ac.in

Abstract: The popular histogram equalisation (HE) technique, which was developed to improve the image contrast, sometimes may also be misused to hide intensity variations in tampered images with ill intention. The authors investigate how existing image forensic techniques may fail to detect HE operation in highly compressed and low-resolution images. They then propose an algorithm to detect whether a given image (either uncompressed or JPEG compressed) has undergone the HE process or not. It is based on the frequency domain analysis of image histogram and exploits the difference in DC and AC coefficients in histogram's discrete Fourier transform. It can detect HE operation even if the image is saved in JPEG format after the equalisation, where most the existing algorithms fail. The extensive computer simulations over large dataset show the effectiveness of the proposed algorithm.

1 Introduction

1.1 Motivation

In the modern digital era, the availability of low cost and powerful image editing softwares (e.g. Adobe Photoshop, CorelDraw etc.) and tools have made the task of image editing so simple that even an unexperienced person can edit, manipulate and process images without leaving any visual clues. These days, as a huge population of the world relies on images and videos shared very frequently through social media platforms such as Facebook, WhatsApp, Snapchat, and Instagram, which may be used for propagating wrong information through tampered/modified images and videos. Thus, from the information security viewpoint, authentication of digital images and videos is the need of the time and multimedia forensics has emerged as a significant research area. The primary goal of digital image forensics is to identify the nature of manipulation or tampering done in the image. Since it is impossible to detect all types of forgeries with a single method, a number of methods have been proposed to detect image alterations under different scenarios [1–4].

The image authentication approaches, in general, can be classified into two broad categories: active and passive [5]. In digital watermarking [6–9], one of the most popular active approaches, the watermark is embedded into the image either at the time of image generation or before any processing. In contrast, however, the passive methods [10–15] do not need any prior information for the analysis of the image and thus makes a blind decision. The wide applicability and practicality have made the passive forensic analysis as one of the popular research fields. Over the past few years, several passive forensic techniques have been proposed. For instance, in [16], authors have developed a forensic method by detecting traces of resampling. The lighting inconsistencies [17], colour filter array aberrations [18], as well as the noise patterns in camera sensors [19] have been used to identify tampered regions in images. In [20], using multiple hypothesis testing, authors proposed a unique approach revealing the order of operations that have been performed over image.

Recently, due to its wide acceptability, the forensic issues related to JPEG compressed images has received a great attention. Many algorithms have been developed to determine whether a given JPEG image is doubly compressed or not [21–25]. These methods consider double compression as a possible indication of forgery; however, sometimes, images may simply be decompressed

and recompressed again without any manipulation, just to satisfy the file-size limitations of uploading. A number of anti-forensics techniques, such as [26–29], have been developed to dodge existing forensics methods, but at the same time there has been a continuous effort to develop algorithms to cope up with such anti-forensic methods [30].

It has been observed that often image forgery operations are followed by some filtering and enhancement techniques to hide the traces of manipulations and to give more realistic look to the forged images. The popular image processing operations such as edge sharpening, gamma correction, histogram equalisation (HE), noise reduction and median filtering, developed mainly for image enhancement, may also be used as a means to hide image manipulations. For example, Fan *et al.* [31] proposed an image enhancement operation based on variational deconvolution of the image and suggested that the same can be used as anti-forensic operation to disguise the traces of other image processing operations. Thus, revealing the traces of these operations may be very important in many forensic applications. In this paper, we develop a technique to detect whether the given image (uncompressed or JPEG compressed) is histogram equalised or not. It should be emphasised here that although detecting specific operation (HE in this paper) may not necessarily guarantees a malicious tempering, it definitely creates some uncertainty about the originality of the image.

1.2 Related works

In recent past, many methods to a detect specific operation performed over images have been proposed in [32–36]. For example, Zhang *et al.* [32] have used high-order local ternary patterns to detect non-linear median filtering operation. Kang *et al.* [33] have proposed the use of autoregressive model to reveal the traces of median filtering operation. Similarly in [34], a method to jointly detect the filtering and JPEG compression operations in digital images has been proposed. Apart from median filtering, contrast enhancement is another important operation generally used to hide the traces in tampered images (particularly to hide intensity irregularities occurred due to image manipulations), and has been explored for forensic applications [35, 36].

In [35], technique which detects HE by measuring the strength of high-frequency components in image's histogram has been proposed. This is based on the assumption that unaltered images

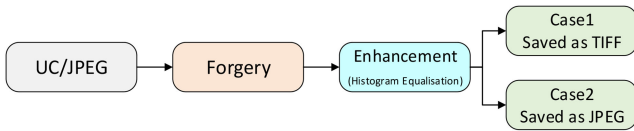


Fig. 1 Different scenarios in which forged images may be saved

(without contrast enhancement) generally have a smooth contoured histogram. However, this assumption of smooth contoured histogram of unenhanced images may not be always valid. We have observed two such cases in which this assumption fails. Firstly, the unaltered low-resolution (small sized) images exhibits discontinuities in their histogram, as all pixel intensities (within dynamic range) may not be present in such images. Secondly, when images are heavily compressed, many of the intensities may be mapped to single intensity due to their quantisation to achieve high compression, thereby resulting in a histogram with unsmooth contour. In [36], Cao *et al.* proposed a method to detect contrast enhancement by comparing the number of zero-height-gap (non-occurring intensities) in the histograms of altered and unaltered images against a threshold. This method outperforms Stamm's [35] method at the low quality of JPEG compression. Although, this method works well for large-size images but has poor accuracy for small-size (or low resolution) images. One of the reason of performance degradation for small-size images is due to the fact that an unaltered small-size image itself has a number of empty bins in its histogram. It may be noted that low-resolution images (as small as 16×16 or 8×8) are used in many applications. For example, in copy move forgery generally, a small patch is copied and pasted in images to hide or add some information. Furthermore, small-size images are used as icons or thumbnail representation.

Another major drawback of methods developed for contrast enhancement-based forensics [35, 36] is that they assume that the contrast enhancement operation is the last step of manipulation applied to the images. These state-of-the-art methods fail to detect contrast enhancement operation if image is JPEG compressed after the enhancement. However, very few forensic methods have been developed for images that are post processed after the compression. For instance, in [37], Conotter *et al.* developed a method to reveal the entire chain of operations, which can detect linear filtering operations in between two JPEG compressions. In [38], Chen *et al.* proposed a blind technique to detect the median filtered image. This method [38] even sustains strong post-processing operation. To the best of our knowledge, no attempts have been made to perform forensic detection of HE (one of the most popular contrast enhancement technique) process on images saved in JPEG format after the HE process, which is the main objective of this paper.

1.3 Contributions

The objective of this paper is to develop an efficient method to detect whether the given image (uncompressed or JPEG compressed) has undergone through HE operation or not. We further aim that proposed method should perform satisfactorily even for low resolution (small size) images, where most of the previously developed methods [35, 36] fail. The main contributions of this work can be summarised as follows:

- In this paper, first we would try to unfold the reason that why most of the existing methods developed for detecting HE operation in images [35, 36] have poor performance for low-resolution images and also why they fail if the image is JPEG compressed after equalisation. Specifically, we will analyse the histogram of images at different resolutions to demonstrate that the assumption of a smooth contoured histogram of un-equalised images or non-occurrences of zero in original images fails for low resolution and heavily compressed images (Sections 2.2 and 2.3).
- Based on our analysis, we target to detect HE images (even low-resolution images) in two different scenarios (Case I and Case II of Fig. 1). For Case I, the HE image is saved in an uncompressed format (such as TIFF, BMP, PNG), while Case II

represents the case when the equalised image is JPEG compressed (post processed). Present techniques [35, 36] are limited to the Case I only and fails if the equalised image is saved in JPEG format. The proposed method exploits frequency domain characteristics of the image histogram to determine if the given image (either in uncompressed or JPEG format) has been HE or not (Section 3).

1.4 Organisation

The rest of this paper is organised as follows. Section 2 reviews the HE technique and its effect on the histogram of an equalised image saved in uncompressed and compressed formats. Further, this section analyses the histograms of low-resolution images and that of highly compressed images and unfolds the reasons that why the assumption of a smooth contour of unequalised images may not be always valid. In Section 3, we propose a novel algorithm to detect HE images in different scenarios. The experimental results are presented in Section 4. Finally, the paper is concluded in Section 5.

2 Review of HE and effects of various operations on histogram

Since paper focuses on detection of HE process in images, we will briefly review the HE technique. The HE process redistributes pixel intensities in such a way that processed image has almost a flat histogram. As the detection of HE process is mainly based on exploiting histogram characteristics, it is important to study the effects of various operations on the image histogram. Therefore, in this section we also analyse the dependency of smoothness of histogram on image resolution and degree of compression.

2.1 Histogram equalisation

HE is a one of the most widely used contrast enhancement technique, which transforms the input histogram (normalised histogram is the probability distribution function) into uniformly distributed output histogram. The histogram of processed image is uniformly spread in the entire dynamic range of pixel intensities [39]. The transformation function for HE is defined mathematically as

$$y_k = T(x_k) = \sum_{i=0}^k p_x(x_i) = \sum_{i=0}^k \frac{n_i}{n}; \quad k = 0, 1, 2, \dots, L-1 \quad (1)$$

Here, variable x represents the pixel intensities of input image that is to be enhanced and y is the output value for each input x to the transformation T , n_i is the number of pixels with i th intensity, n is the total number of pixels in the image and L is the number of possible intensity levels ($L=256$ for grey-scale images). It must be noted that the discrete transformation in (1) not necessarily provides a perfect uniform probability distribution function. However, it has the general tendency of spreading the histogram of the input image in such a way that the histogram of equalised image spans over the full range of intensities [39]. This spreading and intensity redistribution property of HE process may sometimes be used as a tool to hide the traces of image tampering.

Fig. 2a shows the histogram of original 'Lena' image and Fig. 2b depicts the histogram of its equalised version. It can be observed from Fig. 2b that HE causes almost even spread in the histogram and also results in a large number of empty bins in it. In previous works such as [36], this property of increased number of empty bins in histogram of equalised images is used as an evidence to reveal HE operation in images saved in uncompressed formats like TIFF and BMP. However, when an equalised image is saved in JPEG format, it is difficult to detect HE operation on the basis of the number of empty bins, as evident from Fig. 2c showing the histogram of equalised Lena image but saved in JPEG format with quality factor (QF)=75 and having lesser number of empty bins (the same has been described in more detail in Section 2.3). It must be noted that although after JPEG compression there is a redistribution of pixel values in image histogram, the overall

contour of histogram still remains almost uniform. In subsequent sub-sections, we will show that unsmooth histogram with large number empty bins may occur in low-resolution images and highly compressed images, even without the HE.

2.2 Effect of image resolution on histogram

As mentioned earlier, the previous works [35, 36] used the histogram of images to reveal traces of enhancement operations by assuming that unequalised images have their histogram with smooth contour, while histogram of equalised images shows an increase in the number of empty bins. However, we observed that histogram of small-size unequalised images also exhibit similar characteristics. In order to verify our observation, we consider original 'Elaine' image and its downsampled versions at six different resolutions (of sizes 256×256 , 128×128 , 64×64 , 32×32 , 16×16 and 8×8). Histogram of the image at different resolutions is shown in Fig. 3. A close observation of Figs. 3a–f reveals that the contours of histograms of low-resolution unequalised images are not as smooth as that of the high resolution. Further, it can be observed that the histogram of low-resolution images has many empty bins, which causes irregularities (unsmoothness) in histogram's contour. This observation can be justified by the fact that for small-size images, the total available pixel values are not enough to cover the entire range of the histogram thereby resulting in zero-valued bins in the histogram. Thus, the assumption of a smooth contoured histogram of unequalised images, which is the basis of earlier studies [35] is not a valid for small-size (low resolution) images. The tampered region, in many forensic scenarios, maybe just a small patch, for example, some number/characters or the face of a person etc. In such cases, these existing methods would usually fail.

2.3 Effect of compression on histogram contour

In order to reduce bandwidth requirement for transmission over the Internet/mobile networks or to satisfy the file-size limitations for uploading, many times images need to be highly compressed. This is generally achieved through the use of large step-size quantiser, which causes unsmoothness in the contour of image histogram. Since JPEG is widely used for compression of images shared over social media, we consider JPEG compressed images to study the effect of compression (or quantisation) on image histogram. In JPEG compression, DCT coefficients are quantised by dividing them with corresponding elements of a predefined quantisation matrix Q . The elements of Q matrix are scaled according to the QF. For a specified QF, elements of matrix Q are generally large for high-frequency coefficients compared to the DC and low-frequency coefficients. To achieve a high degree of compression, more and more high-frequency DCT coefficients are quantised to zero value according to

$$Y(u, v) = \text{round}\left(\frac{F(u, v)}{q(u, v)}\right) = 0; \quad \text{if } q(u, v) > 2F(u, v) \quad (2)$$

where $Y(u, v)$ is the quantised version of DCT coefficient $F(u, v)$ and $q(u, v)$ is the corresponding element of the quantisation matrix. As indicated in (2), $Y(u, v)$ will be rounded to zero if $q(u, v)$ is greater than twice the magnitude of $F(u, v)$. Since at lower value of QF (high degree of compression), most of the elements in quantisation matrix are of large magnitude, many DCT (mainly high frequency) coefficients are likely to be quantised to zero value. Due to loss of these high frequency coefficients, the reconstructed image appears to be relatively smoother (containing only low-frequency components) compared to images compressed at higher QF. That is, in a highly compressed image, the majority of pixels within the neighbourhood of a given pixel are likely to be of similar intensity. Thus, the histogram of highly compressed images will show many sudden peaks and discontinuities as a result of which Stamm's [35] method fails for low quality of compression (the same fact has been established in Cao's [36] work). It must be noted that till now the QF refers to the primary quality of compression that is the QF_1 at which image is

compressed before equalisation. Now in order to understand the effect of post compression (Case II), in Fig. 4 we plot the cumulative distribution of 'E' (energy parameter defined and used in Stamm's [35] work) is computed for uncompressed, equalised (Case I) and equalised plus JPEG compressed (Case II, $QF_2 = 75$) versions of 1338 images from UCID [40] database. It can be observed from Fig. 4 that the distribution of 'E' for original images and its equalised version only are much separated and thus can be differentiated using an appropriate threshold. However, for the equalised plus JPEG compressed images, the parameter 'E' follows the same distribution curve as original images. Hence, Stamm's method is limited to Case I only and fails for Case II.

As mentioned earlier (see Fig. 2), HE operation results in almost uniformly distributed histogram over the full intensity range and increases the number of zero height (or empty) bins in the histogram. The algorithm proposed in [36] is based on the number of these empty bins in image histogram, which is compared with a pre-determined threshold value to decide if the given image is HE or not. It works well for large-size images, but has poor accuracy for low-resolution images. This is mainly due to the fact that the non-equalised small-size images themselves have a lot of empty bins in their histogram (Fig. 3). In order to further strengthen the fact that the empty bins in the histograms are not only due to HE operation performed on the image but also depends on the size of (unequalised) image and JPEG compression after the equalisation process, we have carried out an experiment considering 1338 images, each of size 512×384 , from the UCID database [40]. The small-size images, of six different resolutions 256×256 , 128×128 , 64×64 , 32×32 , 16×16 and 8×8 are then generated by down-sampling, thereby resulting in a database of $9366 (= 1338 \times 7)$ images, including the original images. The number of empty bins in image histograms of original and HE images of different resolutions are then counted. Fig. 5 shows the average number of empty bins (averaged over the number of images of a particular size) in the histograms of unequalised and uncompressed images (UC), their JPEG compressed ($QF = 75$) versions (JPEG), images obtained after HE of uncompressed images (UC + HE), HE of JPEG ($QF = 75$) compressed images (JPEG + HE), and images which are JPEG compressed after equalisation (HE + JPEG). It can be observed from Fig. 5 that the average number of empty bins in the histogram equalised images (irrespective whether images are initially uncompressed or JPEG compressed, i.e. UC + HE and JPEG + HE cases) is very high and is almost independent of image size. However, the average number of empty bins in unequalised images (UC and JPEG cases) increases as the image resolution decreases, and approaches to almost same values as that of histogram equalised images, for 16×16 and 8×8 size images. Furthermore, it can be observed that for histogram equalised images saved as JPEG (HE + JPEG case), the number of empty bins increases as image resolution decreases. Therefore, it is obvious that simply counting the number of empty bins, as suggested in [36], is not sufficient to discriminate unequalised and histogram equalised images, particularly for small-size images (Case I) and for the cases where the equalised image is saved in JPEG format (Case II).

The above arguments justify our observations that the assumption of the smooth histogram is not valid for low-resolution images (Section 2.2) and for highly compressed images (Section 2.3), which was the basis of previous studies [35]. Also, Cao's [36] method, although independent of primary quantisation (QF_1), is limited to large resolution images only. In Section 2.3, we also showed that both Stamm's [35] and Cao's [36] methods are designed to work in the Case I (Fig. 1) scenario only and fails if the image is JPEG compressed after equalisation (Case II, Fig. 1). In the following section, a novel algorithm is designed to detect HE process in an image that works satisfactorily irrespective of image resolution and image format.

3 Proposed method for identifying histogram equalised images

In this section, we propose a very generic method to detect HE process in image, which is based on the frequency domain features

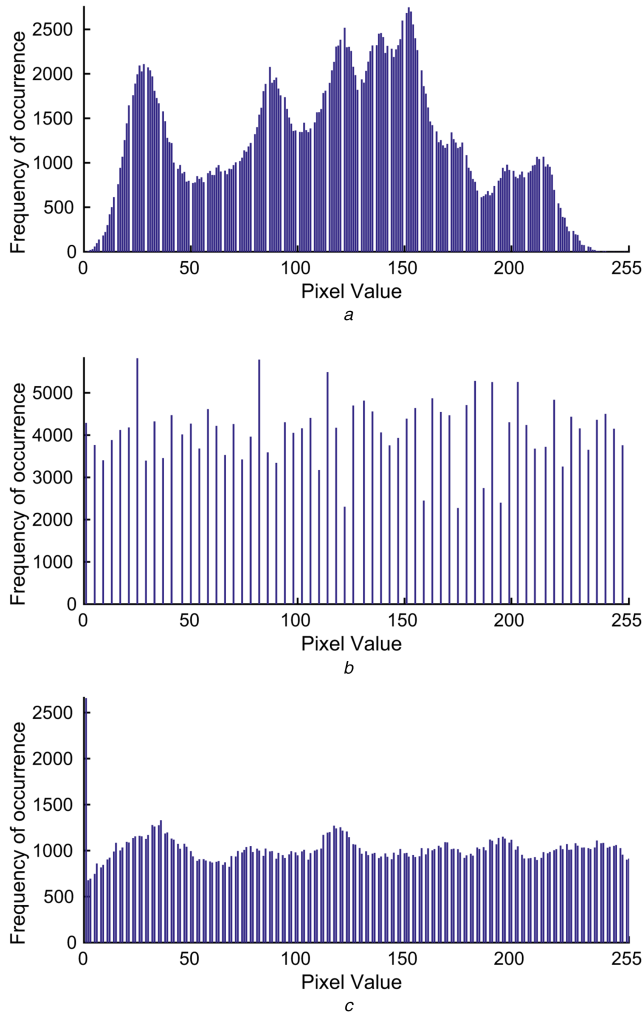


Fig. 2 Histogram

(a) Original Lena image, (b) Its equalised version, (c) Its equalised plus JPEG compressed version

of the images histogram and is able to reveal the traces of HE even if the equalised image is JPEG compressed (i.e. it works for both Case I and Case II of Fig. 1).

3.1 Discrete Fourier transform (DFT) of image histogram

An image histogram is the representation of frequency of occurrences of grey-scale intensities in the image, and can be considered as a 1D discrete signal (with intensity as an independent variable and count of intensity as a dependent variable). The information about the degree of changes (or frequency of abrupt changes) in the histogram can be obtained by transforming histogram in frequency domain. For an 8-bit grey-scale image I , with pixel intensities varying in the range $n = 0, 1, 2, \dots, 255$, and if $H(n)$ represents count of n th intensity level, then N point (here $N = 256$) DFT of the histogram H can be defined as

$$X(k) = \sum_{n=0}^{N-1} H(n) \exp\left(-\frac{j2\pi nk}{N}\right); \quad k = 0, 1, \dots, N-1 \quad (3)$$

where N represents the number of equally spaced points in the interval $[0, 2\pi]$ on a unit circle in the Z -plane. Since $H(n)$ is a real valued discrete sequence, its DFT $X(k)$ will be a complex quantity and will exhibit complex conjugate symmetry. Thus, for a real N -point discrete time 1D signal $H(n)$, from (3), it can be easily verified that

$$X(N-k) = X^*(k) = X(-k) \quad (4)$$

Consequently

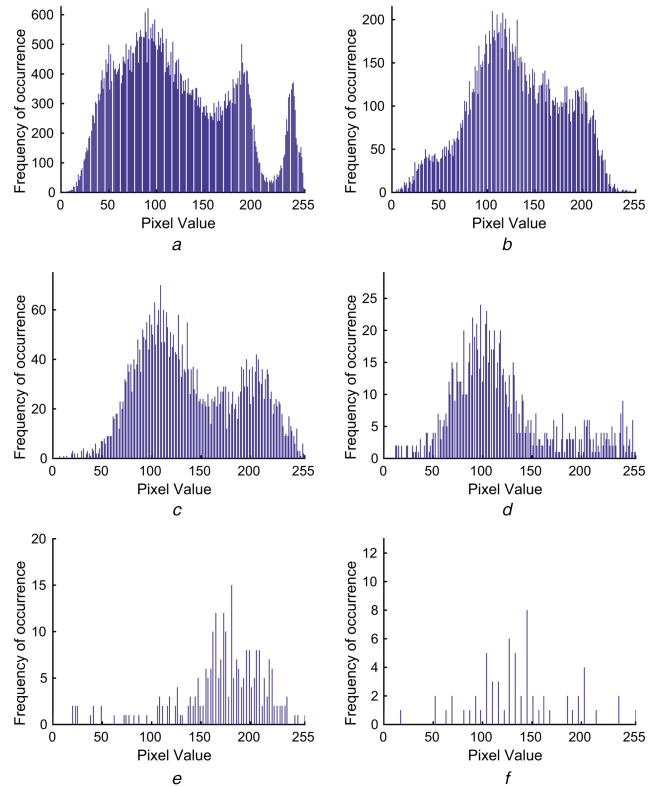


Fig. 3 Histogram of Elaine image at resolutions

(a) 256×256 (b) 128×128 (c) 64×64 (d) 32×32 (e) 16×16 (f) 8×8

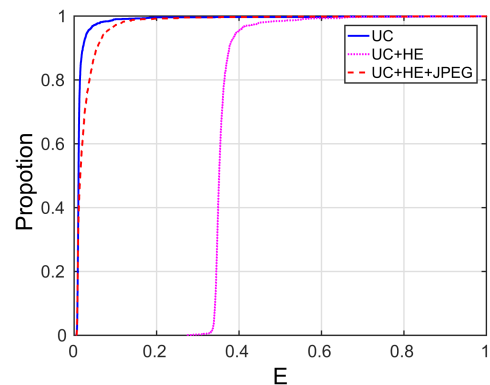


Fig. 4 Cumulative distribution of 'E' values (Stamm et al. [35]) computed from UCID images, its histogram equalised version (Case I) and equalised plus JPEG compressed (Case II) version

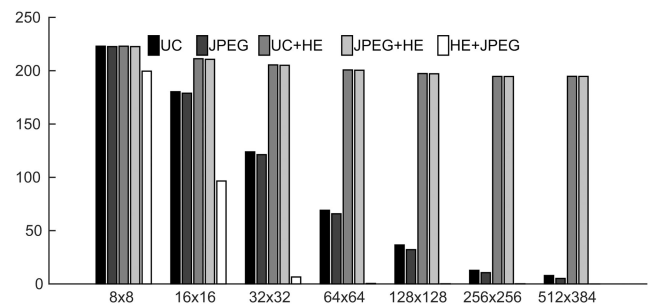


Fig. 5 Average number of empty bins in images at different resolutions

$$|X(N-k)| = |X(k)| \quad (5)$$

Therefore, from (4) and (5), it can be inferred that for an even N (which is the case here), apart from a DC term ($X(0)$), the magnitude of $X(k)$, i.e. $|X(k)|$ will have only $N/2$ unique values which are symmetrically located on both sides of $k=N/2$. The proposed algorithm uses frequency domain characteristics of histogram of given image to detect HE operation on it.

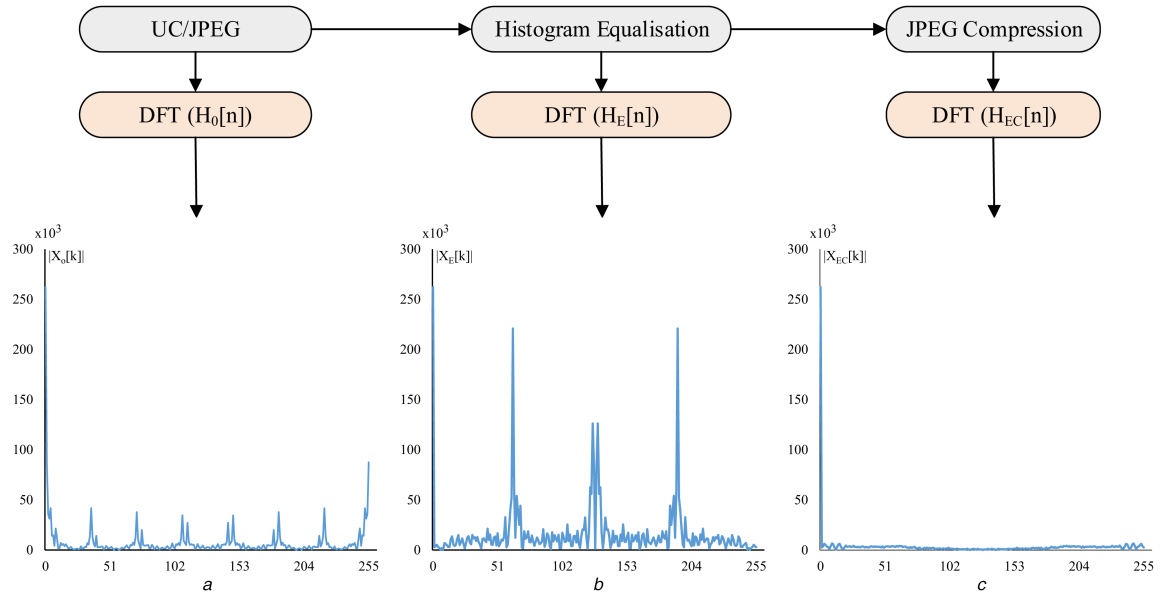


Fig. 6 Block diagram of the considered framework

(a) Magnitude plot of the DFT of greyscale histogram of an original unequalised image. (b) Magnitude plot of the DFT of greyscale histogram of the equalised version of the image. (c) Magnitude plot of the DFT of greyscale histogram of an equalised then compressed image

3.2 Proposed algorithm

In order to describe the proposed algorithm, consider that an unequalised original image I_o (which may be either uncompressed or JPEG compressed) has undergone the HE process followed by JPEG compression, resulting in images I_E and I_{EC} , respectively. Let H_o , H_E and H_{EC} are the histograms of I_o , I_E and I_{EC} images, respectively. We believe that exploiting the frequency domain information inherent in the processed (HE process in our case) images, the nature of the process applied to generate the corresponding image can be identified. Let $X_o(k)$, $X_E(k)$ and $X_{EC}(k)$ are DFT coefficients of H_o , H_E and H_{EC} obtained using (3), respectively.

The magnitude spectrum of histograms of a typical unequalised (uncompressed or JPEG compressed) ($|X_o(k)|$), HE image ($|X_E(k)|$) and JPEG compressed equalised image ($|X_{EC}(k)|$) are shown in Figs. 6a–c, respectively. In each $|X(k)|$, $k=0$ represents the corresponding DC term and can be written as $|X(0)| = \sum_{n=0}^{N-1} H(n)$, where H is the histogram whose DFT is to be evaluated. It may be noted that $|X(0)|$ is equal to the total number of pixels in the image, which will remain the same before and after the HE and/or JPEG compression. That is, $|X_o(0)| = |X_E(0)| = |X_{EC}(0)|$, which is also evident from Figs. 6a–c. Further, it can be observed that the maximum value in each of the magnitude spectrum plots are the corresponding DC values at $k=0$. All other values in $|X(k)|$ (except at $k=0$) represent different AC components. As mentioned earlier, DFT of histograms (being real 1D data) shall exhibit even symmetry at $k = N/2 = 128$, and is clearly evident from Figs. 6a–c.

We propose to identify the HE process in an image by observing the difference between DC coefficient ($|X(0)|$) and weighted sum of unique AC coefficients ($|X(k)|$; $k \in \{1, 128\}$) of DFT of its histogram. As evident from Fig. 2a, the histogram of an unequalised image likely to have random envelope, with many abrupt changes in its shape, and therefore corresponding $|X(k)|$; $k \in \{1, 128\}$ are likely to have larger values, which can be verified in Fig. 6a. Since it is expected that the HE process generates an image having almost uniformly distributed histogram, and therefore the values of $|X(k)|$; $k \in \{1, 128\}$ are likely to be zero (or very small value). The similar observations can be made for an image which is JPEG compressed after HE as shown in Fig. 2c. This is because, when an equalised image is JPEG compressed, resulting in redistribution of pixel intensities in its histogram; however, the overall contour of the histogram still remains almost uniform (as discussed in Section 2.1, and also evident from

Fig. 2c). Therefore, in histogram equalised images, the AC coefficients are expected to be much smaller as compared to DC coefficient. However, in practice the histogram of equalised image is not perfectly uniform and often contains sudden jumps or breaks, which may sometime results in large value of mid and high-frequency components in its DFT. To overcome this problem, we suggest to use weighted sum of AC coefficients, with weights decreasing exponentially with frequency. Therefore, the difference between DC and weighted sum of AC coefficients in histogram's DFT may be used as feature to identify the HE process in images. The AC coefficients should be weighted in such a way that low-frequency components are emphasised more than the mid and high-frequency components.

Based on above discussions and using the DFT coefficients of the histograms, we propose that the DC normalised difference between DC and weighted sum of AC coefficients of DFT of the image histogram can be used to identify whether the given image is histogram equalised or not. For this purpose, we define a new parameter ξ as

$$\xi = \frac{|X(0)| - \delta}{|X(0)|} = 1 - \frac{\delta}{|X(0)|} \quad (6)$$

where δ is the weighted sum of magnitude of AC coefficients as defined in (7) and weights are decaying exponential with β as a decay factor

$$\delta = \sum_{k=1}^{128} |X(k)| \exp(-\beta(k-1)) \quad (7)$$

The purpose of β is to deemphasise mid- and high-frequency components. Experiments show that $\beta = 1$ is appropriate.

Since unequalised (uncompressed or JPEG compressed) images have relatively larger values of $|X(k)|$; $k \in \{1, 128\}$ and therefore for such images parameter ξ (defined in (6)) will be of smaller value as compared to that for histogram equalised as well as JPEG compressed images. In order to justify our claims, we have considered 1338 images from UCID [40] dataset and their downsampled versions. Each of these images is histogram equalised and then JPEG compressed with QF=75. For each image, the parameter ξ was evaluated. The mean (μ_ξ) and standard deviation (σ_ξ) of parameter ξ of unequalised (original), histogram equalised and equalised plus compressed images of different sizes are listed in Table 1. It can be observed from Table 1 that the value of μ_ξ is small for unequalised (original) images compared to that of

```

Initialization:
I ← Input Image
H ← Histogram
X ← DFT of H

for each Input Image I do
  for each grayscale value P ∈ {0, 1, ..., 255} do
    | HI(P) = count occurrence of P
  end
  XI ← DFT(HI)
  compute ξ using Eq.6
  if ξ ≥ ξTh then
    | I :Histogram Equalized
  end
end
end

```

Fig. 7 HE detection

only equalised as well as equalised and JPEG compressed images. This ensures that the proposed method can differentiate unequalised and equalised images irrespective of the format in which final image is saved. Additionally, the standard deviation σ_{ξ} of equalised plus compressed images is smaller compared to that of equalised only images. Furthermore, it can be observed that both μ_{ξ} and σ_{ξ} are almost independent of image size. This property ensures that the proposed method can be applied to even low-resolution images, where most of the existing techniques fail. Thus, by comparing the value of parameter ξ of the given image I with a pre-determined threshold (ξ_{Th}), the image can be classified as unequalised or histogram equalised. The proposed algorithm is summarised in Fig. 7.

4 Simulation results and discussion

4.1 Dataset

To test the efficacy of the proposed methods, we have considered two popular standard image datasets, namely UCID [40] and NCID [41]. We select all 1338 uncompressed images (each of size 512×384) from UCID and random 2000 uncompressed images (each of size 256×256) from NCID. In order to demonstrate the effectiveness of the proposed method irrespective of the image size, the low-resolution images are generated by central cropping (CC) as well as down-sampling (DS) all original images to generate images of sizes 8×8 , 16×16 , 32×32 , 64×64 , 128×128 and 256×256 which gives a total dataset of 39,394 ($1338 \times 13 + 2000 \times 11$) uncompressed images. All these images are histogram equalised and are saved in either TIFF or JPEG formats. The accuracy of proposed methods is measured in terms of true positive rate (TPR) and false positive rate (FPR). Here, TPR is defined as percentage of equalised images detected as equalised (true detection), whereas FPR is the measure of the percentage of unequalised images detected as equalised images (false detection). The performance of proposed method is compared with that of Stamm's [35] and Cao's [36] methods. The proposed and other algorithms are simulated using MATLAB2016 and are executed on a workstation with 8 GB RAM and Intel Core i7-6700 at 3.40 GHz \times 8 CPU.

4.2 HE detection

4.2.1 Experiment 1: To measure the detection accuracy (detection of HE process in the given image) of proposed method and to compare with that of Stamm's [35] and Cao's [36] methods, the receiver operating characteristic (ROC) curves (Fig. 8) are generated on UCID dataset [40]. Here, detection ROC curve for Case I (of Fig. 1) corresponding to $QF_1 = 100, 70, 50$ are shown in Figs. 8a–c, respectively. While detection ROC curve for Case II corresponding to $QF_1 = 100, 70, 50$ are shown in Figs. 8d–f, respectively. These curves following observations can be inferred:

- For Case I (equalised images saved in TIFF format), it can be observed from Figs. 8a–c that both the proposed and Cao's [36] methods perform well irrespective of the value of primary QF_1 .

However, the performance of Stamm's [35] degrades as the value of QF_1 decreases or as compression is changed from high quality to the low quality.

- Further, it can be observed from Figs. 8d–f that the proposed method outperforms other contemporary methods [35, 36] in detecting the HE process in the JPEG images (Case II). Further, it may be emphasised that the proposed method achieves high TPR under low FPR value, whereas other two compared methods [35, 36] totally failed to detect HE operation. These results justify out initial observations mentioned in Section 2.3.

4.2.2 Experiment 2: In order to evaluate the identification accuracy of different methods for low-resolution images and at different secondary QF_2 (the QF of JPEG compression performed after the equalisation), another experiment on the dataset mentioned in Section 4.1 is performed. First the images of different size in the dataset are histogram equalised. Then the equalised images are saved as uncompressed TIFF format (referred as UC) as well as JPEG compressed at $QF_2 = \{10, 30, 50, 75, 90, 100\}$. In other words, UC is representing Case I and JPEG compressed images represent Case 2 of Fig. 1. This gives us a total of 275,758 ($7 \times 39,394$) images. The accuracy of the proposed and other existing methods is listed in Table 2 (for image size 512×384 , 256×256 , 128×128 and 64×64) and Table 3 (for image size 32×32 , 16×16 and 8×8) for different values of QF_2 . Here, the accuracies are reported in terms of TPR for a fixed value of FPR (1%). For the proposed method, the threshold values obtained are 0.8473, 0.8437, 0.8139, 0.8325, 0.8235, 0.8327, 0.8576 for image size 512×384 , 256×256 , 128×128 , 64×64 , 32×32 , 16×16 and 8×8 , respectively. It must be noted that we have performed evaluation on small-size images generated by both central cropping and downsampling of the original images. Centrally cropped (CC) images, in contrast to downsampled images (DS), does not preserve the overall structure of the actual image. However, since in copy and move forgery, a cropped portion of the image is generally used to hide or add some data, we have performed the evaluation on centrally cropped images also.

It can be observed from Table 2 and Table 3 that for case I, Stamm's method [35] has almost 100% accuracy for image size up to 32×32 , and the performance of Cao's method [36] degrades drastically for small-sized images; however, the proposed method has accuracy consistently more than 96% irrespective of the image size. Similarly for Case 2, the proposed method completely outperforms both methods [35, 36] under consideration. The poor performance of Stamm's [35] and Cao's [36] is mainly due to the quantisation effect (during JPEG compression/decompression) as discussed in Sections 2.2 and 2.3. In contrast, the proposed method uses feature in frequency domain (DFT of histogram), and mainly exploits the flatness in histogram (before and after the equalisation). Since, the algorithm suppresses the effect of sudden peak and gaps in the histogram by penalising mid- and high-frequency components, the proposed method performs well even if equalised image is JPEG compressed. It must be noted that for small size (16×16 , 8×8) and highly compressed ($QF = 10$) images, all these algorithms fail to detect HE operation. This is because, heavy compression on very small size images results in the complete loss of the structure of the image. In fact, such images are of no practical use.

4.2.3 Experiment 3: In order to verify that the proposed image works equally well for large-size images, we perform another experiment randomly selected 2500 images from the popular RAISE [42] image dataset. The dataset mainly consists of outdoor, indoor, landscape, natural, people, object and building images, each of size 4928×3264 .

From the ROC curve shown in Fig. 9, it can be observed that although both Cao's [36] and Stamm's [35] methods have slightly better performance compared to proposed method for Case I (when equalised image saved in uncompressed format). However, for Case II, when equalised image is saved in JPEG format, the

Table 1 Average value (μ_{ξ}) and standard deviation (σ_{ξ}) of ξ for unequalised (O), equalised (E) and equalised plus compressed (EC) images of different size

Size	$\mu_{\xi}(O)$	$\sigma_{\xi}(O)$	$\mu_{\xi}(E)$	$\sigma_{\xi}(E)$	$\mu_{\xi}(EC)$	$\sigma_{\xi}(EC)$
512 × 384	0.4771	0.1969	0.9712	0.0425	0.9718	0.0417
256 × 256	0.4435	0.2220	0.9727	0.0469	0.9732	0.0455
128 × 128	0.3476	0.2446	0.9754	0.0364	0.9756	0.0354
64 × 64	0.3200	0.2807	0.9719	0.0534	0.9713	0.0508
32 × 32	0.3107	0.2850	0.9686	0.0799	0.9666	0.0755
16 × 16	0.3587	0.2786	0.9636	0.1029	0.9552	0.0969
8 × 8	0.4326	0.2794	0.9466	0.1345	0.9198	0.1237

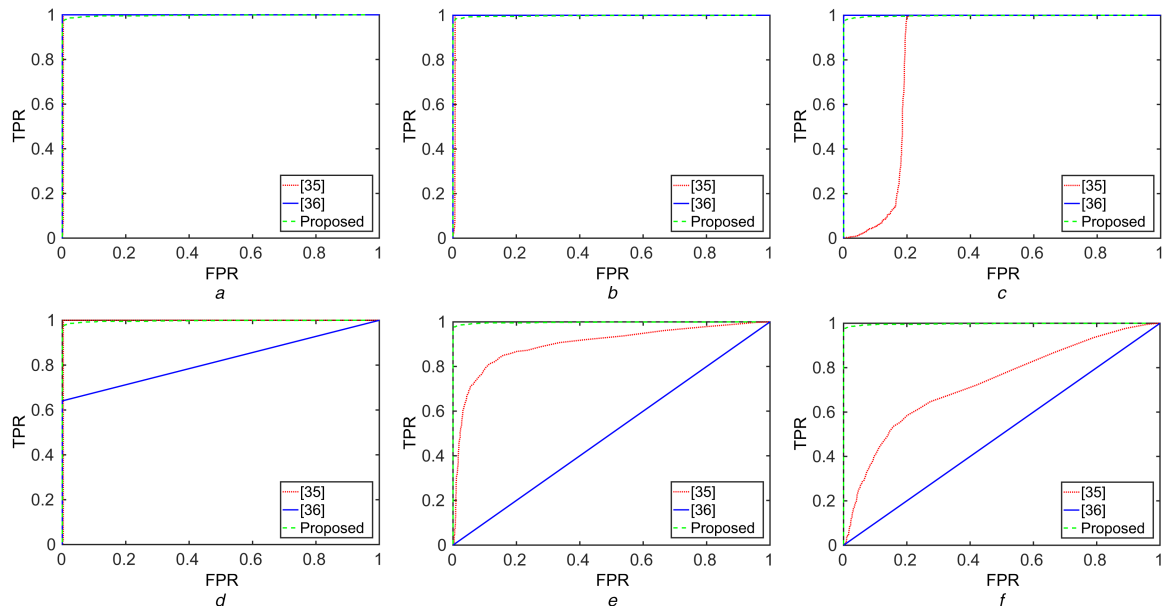


Fig. 8 HE detection ROC curves on Dataset 1 for different combination of QF_1 and QF_2

(a–c) Case I of Fig. 1; (d–f) Case II of Fig. 1. Here, ‘ QF_1 ’ denotes the JPEG QF of image before equalisation, ‘ QF_2 ’ denotes the QF at which histogram equalised image is JPEG compressed and $QF_{1/2} = UC$ means image is saved in uncompressed format (TIFF)

Table 2 Detection accuracy in terms of TPR for a fixed value of FPR = 1% at different values of QF_2 for image size ranging from 512 × 384 to 64 × 64

Case	QF2	Method	512 × 384		256 × 256		128 × 128		64 × 64	
			Original	CC	DS	CC	DS	CC	DS	
1	UC	Stamm [35]	100.00	100.00	100.00	100.00	100.00	100.00	100.00	100.00
		Cao [36]	100.00	100.00	100.00	98.05	99.40	55.39	89.82	
		Proposed	98.05	98.80	98.66	99.33	98.80	98.58	98.80	
2	100	Stamm [35]	100.00	100.00	100.00	100.00	100.00	100.00	100.00	100.00
		Cao [36]	63.47	64.67	65.84	47.16	41.92	5.16	9.66	
		Proposed	98.05	98.80	98.95	99.33	98.80	98.58	98.80	
	90	Stamm [35]	9.73	4.72	5.23	1.57	2.02	1.27	0.82	
		Cao [36]	0.00	0.00	0.00	0.00	0.00	0.00	0.00	
		Proposed	98.05	98.88	98.95	99.40	98.80	98.73	99.03	
	75	Stamm [35]	7.41	3.74	4.12	1.35	1.57	1.12	0.67	
		Cao [36]	0.00	0.00	0.00	0.00	0.00	0.00	0.00	
		Proposed	98.05	98.88	98.95	99.40	98.88	98.88	99.03	
50	Stamm [35]	14.37	13.10	13.02	1.27	3.52	1.35	0.97		
	Cao [36]	0.00	0.00	0.00	0.00	0.00	0.00	0.00		
	Proposed	98.13	98.95	98.95	99.48	98.95	99.03	99.10		
30	Stamm [35]	8.21	4.22	4.22	1.14	2.15	0.98	0.83		
	Cao [36]	0.00	0.00	0.00	0.00	0.00	0.00	0.00		
	Proposed	98.13	98.95	98.95	99.48	98.95	99.03	99.10		
10	Stamm [35]	3.17	3.58	2.54	0.59	1.73	2.41	0.94		
	Cao [36]	0.00	0.00	0.00	0.00	0.00	0.00	0.00		
	Proposed	98.05	98.05	98.05	99.33	93.19	94.54	84.81		

Table 3 Detection accuracy in terms of TPR for a fixed value of FPR = 1% at different values of QF_2 for image size ranging from 32×32 to 8×8

Case	QF_2	Method	32×32		16×16		8×8	
			CC	DS	CC	DS	CC	DS
1	UC	Stamm [35]	100.00	100.00	37.80	100.00	17.59	1.05
		Cao [36]	36.45	76.65	21.18	60.33	0.00	0.00
		Proposed	98.43	99.03	98.05	98.88	96.26	98.58
2	100	Stamm [35]	100.00	100.00	25.15	99.93	10.93	0.22
		Cao [36]	26.50	53.82	22.08	60.25	0.00	0.00
		Proposed	98.43	99.03	98.05	98.88	96.33	98.58
	90	Stamm [35]	0.97	0.07	0.60	0.00	0.52	0.00
		Cao [36]	0.00	0.00	72.46	40.04	1.35	0.00
		Proposed	98.50	99.03	98.13	98.88	96.48	98.65
	75	Stamm [35]	0.90	0.00	0.52	0.07	0.45	0.00
		Cao [36]	0.00	0.00	78.37	28.37	1.12	0.07
		Proposed	98.65	99.10	98.28	99.03	96.63	98.58
	50	Stamm [35]	0.90	0.07	0.60	0.00	0.52	0.07
		Cao [36]	0.07	0.00	75.90	20.81	1.12	0.22
		Proposed	99.10	99.10	98.43	99.25	90.04	92.37
30	Stamm [35]	0.42	0.01	0.33	0.78	0.00	0.10	
	Cao [36]	0.05	0.00	0.01	0.31	0.14	0.00	
	Proposed	98.95	99.10	97.98	98.13	65.42	64.45	
10	Stamm [35]	1.32	0.95	0.30	0.84	0.11	0.11	
	Cao [36]	0.00	0.13	0.00	0.50	0.22	0.27	
	Proposed	89.90	64.82	64.07	25.15	20.96	15.79	

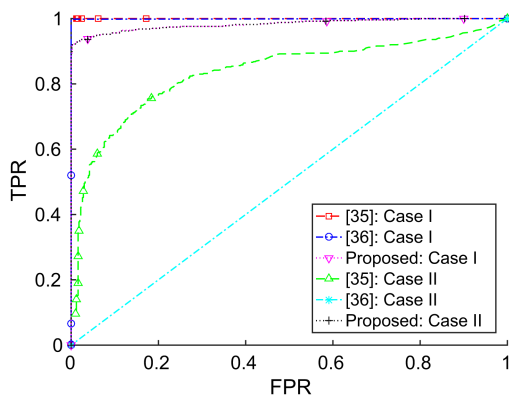


Fig. 9 Detection of ROC curves for large-size images

Table 4 Average computation time (in ms) of proposed and compared methods for images of different size

Size	Stamm [35]	Cao [36]	Proposed
512×384	5.7080	6.9180	3.100
64×64	0.1980	2.0140	0.1440
8×8	0.0800	1.423	0.0670

proposed method outperforms the methods of [35, 36]. Thus our algorithm works satisfactorily both for small-size (as small as 8×8) and large-size images (as large as 4928×3624). Also, it is almost independent of both the primary (QF_1) and secondary (QF_2) QF s of compression, which is a major advantage of the proposed algorithm.

4.3 Computational complexity

To compare the computational complexity of different methods, we measure and compare the average (averaged over number of images) computation time. Table 4 shows the average computation time of different algorithms for different size of images. It can be observed that proposed method is computationally efficient as compared to methods reported in [35, 36]. This is because the proposed method is based on computing DFT of histogram of

images, which consumes lesser time than the features used in [35, 36].

5 Conclusion

In this paper, we proposed an efficient image forensics technique to detect the HE operation which can be used to hide the traces of previous JPEG compression or intensity variation in images due to manipulations. The proposed method is very general and can detect the HE operation in images even if they are post-processed (JPEG compressed) after the equalisation operation. Based on our analysis on the effects of equalisation and compression processes on the image histogram and by observing the frequency domain characteristics of histogram, a new parameter has been suggested and its effectiveness to differentiate histogram equalised images from unequalised images has been demonstrated. Experimental results have shown the efficacy of the proposed methods and demonstrate that the proposed method can detect HE process satisfactorily for low- and high-resolution images. It has also been shown that it can detect HE operation even if the image is JPEG compressed after equalisation, where most of the contemporary methods fail. It may be noted that the proposed method can detect only standard HE process and does not work for more advanced equalisation techniques like contrast limited adaptive histogram equalisation (CLAHE), dynamic histogram equalisation (DHE). In future, we aim to develop similar algorithms for advanced equalisation techniques as well as to identify other image processing operations frequently used to hide image manipulations.

6 Acknowledgments

The authors would like to thank Dr. G. Cao (School of Computer Science, Communication University of China) for sharing the codes of [36] which is used for the purpose of comparisons only. They also thank Dr. T. Guha (Electrical Engineering department, IIT Kanpur, India) for her perceptive and valuable discussions which have helped to improve the quality of the paper. This research is partially supported under DSA-I/SAP project funded by University Grant Commission, Govt of India.

7 References

- [1] Piva, A.: 'An overview on image forensics' (ISRN Signal Processing, 2013)

- [2] Korus, P., Huang, J.: 'Multi-scale fusion for improved localization of malicious tampering in digital images', *IEEE Trans. Image Process.*, 2016, **25**, (3), pp. 1312–1326
- [3] Saito, S., Tomioka, Y., Kitazawa, H.: 'A theoretical framework for estimating false acceptance rate of PRNU-based camera identification', *IEEE Trans. Inf. Forensics Sec.*, 2017, **12**, (9), pp. 2026–2035
- [4] De Natale, F.G., Boato, G.: 'Detecting morphological filtering of binary images', *IEEE Trans. Inf. Forensics Sec.*, 2017, **12**, (5), pp. 1207–1217
- [5] Farid, H.: 'Image forgery detection', *IEEE Signal Process. Mag.*, 2009, **26**, (2), pp. 16–25
- [6] Sarreshtedari, S., Akhaee, M.A.: 'A source-channel coding approach to digital image protection and self-recovery', *IEEE Trans. Image Process.*, 2015, **24**, (7), pp. 2266–2277
- [7] Farhadzadeh, F., Voloshynovskiy, S.: 'Active content fingerprinting', *IEEE Trans. Inf. Forensics Sec.*, 2014, **9**, (6), pp. 905–920
- [8] Su, P.-C., Chang, Y.-C., Wu, C.-Y.: 'Geometrically resilient digital image watermarking by using interest point extraction and extended pilot signals', *IEEE Trans. Inf. Forensics Sec.*, 2013, **8**, (12), pp. 1897–1908
- [9] Wang, C., Ni, J., Huang, J.: 'An informed watermarking scheme using hidden Markov model in the wavelet domain', *IEEE Trans. Inf. Forensics Sec.*, 2012, **7**, (3), pp. 853–867
- [10] Farid, H.: 'Exposing digital forgeries from jpeg ghosts', *IEEE Trans. Inf. Forensics Sec.*, 2009, **4**, (1), pp. 154–160
- [11] Swaminathan, A., Wu, M., Liu, K.R.: 'Digital image forensics via intrinsic fingerprints', *IEEE Trans. Inf. Forensics Sec.*, 2008, **3**, (1), pp. 101–117
- [12] Lin, W.S., Tjoa, S.K., Zhao, H.V., *et al.*: 'Digital image source coder forensics via intrinsic fingerprints', *IEEE Trans. Inf. Forensics Sec.*, 2009, **4**, (3), pp. 460–475
- [13] Akhtar, Z., Khan, E.: 'Identifying high quality JPEG compressed images through exhaustive recompression technique'. Int. Conf. Advances in Computing, Communications and Informatics (ICACCI), 2016, pp. 652–656
- [14] Vazquez-Padin, D., Perez-Gonzalez, F., Comesana-Alfaro, P.: 'A random matrix approach to the forensic analysis of upscaled images', *IEEE Trans. Inf. Forensics Sec.*, 2017, **12**, (9), pp. 2115–2130
- [15] Ulutas, G., Ustubioglu, B., Ulutas, M., *et al.*: 'Frame duplication/mirroring detection method with binary features', *IET Image Process.*, 2017, **11**, (5), pp. 333–342
- [16] Popescu, A.C., Farid, H.: 'Exposing digital forgeries by detecting traces of resampling', *IEEE Trans. Signal Process.*, 2005, **53**, (2), pp. 758–767
- [17] Johnson, M.K., Farid, H.: 'Exposing digital forgeries in complex lighting environments', *IEEE Trans. Inf. Forensics Sec.*, 2007, **2**, (3), pp. 450–461
- [18] Popescu, A.C., Farid, H.: 'Exposing digital forgeries in color filter array interpolated images', *IEEE Trans. Signal Process.*, 2005, **53**, (10), pp. 3948–3959
- [19] Lukas, J., Fridrich, J., Goljan, M.: 'Detecting digital image forgeries using sensor pattern noise'. Proc. SPIE, 2006, vol. 6072, p. 15
- [20] Chu, X., Chen, Y., Liu, K.R.: 'Detectability of the order of operations: an information theoretic approach', *IEEE Trans. Inf. Forensics Sec.*, 2016, **11**, (4), pp. 823–836
- [21] Lukas, J., Fridrich, J.: 'Estimation of primary quantization matrix in double compressed JPEG images'. Proc. Digital Forensic Research Workshop, 2003, pp. 5–8
- [22] Popescu, A.C., Farid, H.: 'Statistical tools for digital forensics', *international workshop on information hiding* (Springer, 2004), pp. 128–147
- [23] Huang, F., Huang, J., Shi, Y.Q.: 'Detecting double jpeg compression with the same quantization matrix', *IEEE Trans. Inf. Forensics Sec.*, 2010, **5**, (4), pp. 848–856
- [24] Bianchi, T., Piva, A.: 'Image forgery localization via block-grained analysis of jpeg artifacts', *IEEE Trans. Inf. Forensics Sec.*, 2012, **7**, (3), pp. 1003–1017
- [25] Pasquini, C., Boato, G., Pérez-González, F.: 'Statistical detection of JPEG traces in digital images in uncompressed formats', *IEEE Trans. Inf. Forensics Sec.*, 2017, **12**, (12), pp. 2890–2905
- [26] Kang, X., Qin, T., Zeng, H.: 'Countering median filtering anti-forensics and performance evaluation of forensics against intentional attacks'. 2015 IEEE China Summit Int. Conf. Signal and Information Processing (ChinaSIP), 2015, pp. 483–487
- [27] Ravi, H., Subramanyam, A., Emmanuel, S.: 'Ace – an effective anti-forensic contrast enhancement technique', *IEEE Signal Process. Lett.*, 2016, **23**, (2), pp. 212–216
- [28] Odebade, A., Welsh, T., Mthunzi, S., *et al.*: 'Mitigating anti-forensics in the cloud via resource-based privacy preserving activity attribution'. 2017 Fourth Int. Conf. Software Defined Systems (SDS), 2017, pp. 143–149
- [29] Sharma, S., Subramanyam, A., Jain, M., *et al.*: 'Anti-forensic technique for median filtering using L1-L2 tv model'. IEEE Int. Workshop on Information Forensics and Security (WIFS), 2016, pp. 1–6
- [30] De Rosa, A., Fontani, M., Massai, M., *et al.*: 'Second-order statistics analysis to cope with contrast enhancement counter-forensics', *IEEE Signal Process. Lett.*, 2015, **22**, (8), pp. 1132–1136
- [31] Fan, W., Wang, K., Cayre, F., *et al.*: 'Median filtered image quality enhancement and anti-forensics via variational deconvolution', *IEEE Trans. Inf. Forensics Sec.*, 2015, **10**, (5), pp. 1076–1091
- [32] Zhang, Y., Li, S., Wang, S., *et al.*: 'Revealing the traces of median filtering using high-order local ternary patterns', *IEEE Signal Process. Lett.*, 2014, **21**, (3), pp. 275–279
- [33] Kang, X., Stamm, M.C., Peng, A., *et al.*: 'Robust median filtering forensics using an autoregressive model', *IEEE Trans. Inf. Forensics Sec.*, 2013, **8**, (9), pp. 1456–1468
- [34] Conotter, V., Comesana, P., Perez-Gonzalez, F.: 'Joint detection of full-frame linear filtering and jpeg compression in digital images'. 2013 IEEE Int. Workshop on Information Forensics and Security (WIFS), IEEE, 2013, pp. 156–161
- [35] Stamm, M.C., Liu, K.R.: 'Forensic detection of image manipulation using statistical intrinsic fingerprints', *IEEE Trans. Inf. Forensics Sec.*, 2010, **5**, (3), pp. 492–506
- [36] Cao, G., Zhao, Y., Ni, R., *et al.*: 'Contrast enhancement-based forensics in digital images', *IEEE Trans. Inf. Forensics Sec.*, 2014, **9**, (3), pp. 515–525
- [37] Conotter, V., Comesana, P., Perez-Gonzalez, F.: 'Forensic detection of processing operator chains: recovering the history of filtered jpeg images', *IEEE Trans. Inf. Forensics Sec.*, 2015, **10**, (11), pp. 2257–2269
- [38] Chen, C., Ni, J., Huang, J.: 'Blind detection of median filtering in digital images: a difference domain based approach', *IEEE Trans. Image Process.*, 2013, **22**, (12), pp. 4699–4710
- [39] Gonzalez, R.C., Woods, R.E.: 'Digital image processing' (Addison-Wesley Longman Publishing, Boston, MA, 2001)
- [40] Schaefer, G., Stich, M.: 'UCID: an uncompressed color image database', *Proc. of the SPIE*, 2003, **5307**, pp. 472–480, doi: 10.1117/12.525375
- [41] Liu, Q., Chen, Z.: 'Improved approaches with calibrated neighboring joint density to steganalysis and seam-carved forgery detection in jpeg images', *ACM Trans. Intell. Syst. Technol.*, 2015, **5**, (4), p. 63
- [42] Dang-Nguyen, D.-T., Pasquini, C., Conotter, V., *et al.*: 'Raise: a raw images dataset for digital image forensics'. Proc. 6th ACM Multimedia Systems Conf., 2015, pp. 219–224